100-GHz Radio and Power Over Fiber Transmission Through Multicore Fiber Using Optical-to-Radio Converter

Toshimasa Umezawa, Pham Tien Dat, *Member, IEEE*, Kenichi Kashima, Atsushi Kanno, *Member, IEEE*, Naokatsu Yamamoto, and Tetsuya Kawanishi, *Fellow, IEEE*

(Top-Scored Paper)

***Abstract*—We designed and fabricated a 100-GHz range integrated photoreceiver with zero-bias operational uni-traveling-carrier photodiode and pseudomorphic high electron mobility transistor amplifier, which performed the roles of photonic power generation and 100-GHz RF signal generation. Using the integrated photoreceiver, high data rate radio- and power-over-fiber transmission through multicore fiber communication was demonstrated. Subsequently, a bit error rate of 1×10^{-3} could be achieved with 12 Gb/s, orthogonal frequency division multiplexing, 16 quadrature amplitude modulation, and an intermediate frequency of 92 GHz. The crosstalk issue in radio- and power-over-fiber transmission through multicore fiber was discussed.**

***Index Terms*—High data rate, multicore fiber, optical-to-radio converter, power over fiber, radio over fiber, UTC-PD.**

I. Introuction

DATA traffic in mobile communication, as well as fixed optical fiber communication, has been increasing year by year. In particular, heavy data traffic is predicted in Tokyo during the 2020 Olympic games and realizing a solution to the challenge of heavy data traffic is an urgent matter. In order to overcome this problem, high data rate, high capacity, and low latency wireless communication links have to be developed immediately as an advanced wireless communication system (5G). Analog radio-over-fiber (RoF) is a promising technology and has great potential to build high data links, such as a 5G network with fixed fiber communication. Since high data rates over 100 Gbps per fiber have already been achieved in fixed fiber communication [1], [2], fiber links should be provided to near end-user points including multi-core fiber systems, and the low latency radio signals [3], [4] converted by a photoreceiver should be launched from many simple antennas in small cells. In the case of large-scale small cell systems in front-haul links, the optical power would be decreased owing to the many optical branches of the small cell systems. Therefore, a highly efficient narrow-band analog photoreceiver is essential. Recently, multi-core fiber technologies, such as 32-core to 36-core fibers, have been studied owing to the increasing data rate and capacity of fixed fiber communication [5], [6]. Using the quadrature phase shift keying (QPSK) and multi-level modulation formats (16-QAM or quadrature amplitude modification) technologies using multi-core fibers, high data rate transmissions in the range of Tbps to Pbps were reported [7], [8]. Another possible application of multi-core fibers is the RoF and power-over-fiber (PoF) transmission, where radio signal and photonic power should be delivered simultaneously [9]. Notably, PoF technology has already been adapted to high voltage power line monitoring systems [10]. Since many power supplies are required for massive antenna units including photoreceivers in populous regions, PoF, which has a good affinity for RoF, is essential and attractive to solve these problems (as shown in Fig. 1).

According to the 5G related papers [11]–[13], the millimeter wave region over 30 GHz will be approved in addition to the microwave region below 10 GHz [14], [15] in order to increase the data rate. Although the band of 60 GHz is very useful and well-known to license-free wireless communication applications, it would result in large atmospheric attenuation [16]. The band of 90–110 GHz is very attractive not only from the perspective of low atmospheric attenuation, but also for the effective use of radio resources.

In this study, we report 100 GHz range RoF and PoF transmission through multi-core fiber, and discuss the crosstalk issues between cores in multi-core fibers. Subsequently, a newly developed uni-traveling-carrier photodiode (UTC-PD) for electric power and simultaneous 100 GHz signal generation, integrated with an enhancement mode 100-GHz pseudomorphic high electron mobility transistor (PHEMT) amplifier was employed in

Manuscript received May 9, 2017; revised June 26, 2017; accepted July 19, 2017. Date of publication July 25, 2017; date of current version February 24, 2018. This work was supported in part by the Japanese Government for "R&D to Expand Radio Frequency Resources" by the Ministry of Internal Affairs and Communications and in part by the MIC/SCOPE #165003010. *(Corresponding author: Toshimasa Umezawa.)*

T. Umezawa, P. T. Dat, A. Kanno, and N. Yamamoto are with the Network Science and Convergence Device Technology Laboratory, National Institute of Information and Communications Technology (NICT), Tokyo 184-8795, Japan (e-mail: toshi_umezawa@nict.go.jp; ptdat@nict.go.jp; kanno@nict.go.jp; naokatsu@nict.go.jp).

K. Kashima is with the Hitachi-kokusai Electric, Inc., Kodaira-shi 187-0012, Japan (e-mail: kashima.kenichi@h-kokusai.com).

T. Kawanishi is with the Network Science and Convergence Device Technology Laboratory, National Institute of Information and Communications Technology (NICT), Tokyo 184-8795, Japan, and also with the Waseda University, Tokyo 169-8050, Japan (e-mail: kawanishi@waseda.jp).

Color versions of one or more of the figures in this paper are available online at http://ieeexplore.ieee.org.

Digital Object Identifier 10.1109/JLT.2017.2731991

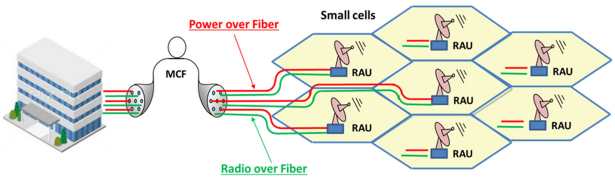

Fig. 1. Schematic illustration of radio- and power-over-fiber transmission through multi-core fiber.

order to reduce the fiber resources required in PoF transmission through multi-core fibers.

II. 100-GHz Optical to Radio Converter Module

A. Configuration of 100 GHz Optical-to-Radio Converter

Regarding conventional ideas using a multi-core fiber, three cores in a multi-core fiber for three biases (for PD, drain and gate biases) would be required in PoF. When a bias free operational high-speed PD can be designed, one of three biases in the cores can be reduced. With the high-speed PD having an electric power generation function, two of three biases in the multi-core fiber can be reduced for PoF as well. A 100 GHz optical-to-radio converter consisting of a zero-bias operational UTC-PD with a range of 100 GHz, InP PHEMT amplifier with a range of 100 GHz, and a bias-T circuit was employed. These components were integrated into a metal package attached to a W-connector. When introducing an optical signal of 100 GHz into the converter, the UTC-PD chip located in the front can perform the roles of generating 100 GHz RF signal current and DC current simultaneously. The RF current and DC current flow through a capacitor and an inductor in the bias-T circuit, respectively. After filtering both currents via the bias-T circuit, the signal of 100 GHz is fed to the input stage of the amplifier, and the DC current is provided to the gate bias through a bias adjustment circuit. The PoF resources can be reduced from three fibers to one fiber (drain bias). Subsequently, two of the fibers can be applied for RoF and PoF transmissions, respectively. Therefore, our design would be advantageous for multi-core fiber based PoF and RoF transmission [17].

B. Zero-Bias Operational 100 GHz Range UTC-PD

A 100 GHz range UTC-PD was designed at 0 V by using only the built-in potential in a p-n junction (see inset in Fig. 2). With the carefully designed carrier concentration and thickness in an InP carrier collector layer and an InGaAs photo-absorption layer, high electron drift velocity of 2×10^7 cm/sec could be obtained at 0 V. By adapting high p-doping level condition in InGaAs and low n-doping level condition in InP, a 3 dB bandwidth of the range of 100 GHz could be simulated with low CR time constant [18], [19]. In the fabrication process, a high mesa structure (5 μm diameter) was formed via dry etching and was buried with polyimide thin film. The ground-signal-ground electrode was also formed for frequency response measurement. The backside illumination structure was employed to enhance the responsivity (0.19 A/W). With on-wafer frequency response probing test at photocurrent of 0.3 mA to 7 mA, a high 3 dB bandwidth of over 110 GHz could be observed at 0 V. Moreover, no difference could be recognized at 1 mA photo-current between the two cases—with (2 V) and without (0 V) bias feed as shown in Fig. 3(a). It indicated that sufficient internal electric field was supplied into the depletion layer, despite applying no bias voltage. Additionally, no difference was observed in the frequency response with various photocurrents (1 mA to 7 mA) at 0 V as shown in Fig. 3(a) and (b), owing to optimum InGaAs doping and thickness conditions. The responsivity was as high as 0.19 A/W. Note that the frequency response was measured from around 15 GHz, in consideration of the stability and line-width (10-MHz) of two DFB laser sources. The vertical axis was normalized as the relative gain. In the low frequency range of 10 MHz to 67 GHz, the flat frequency response could be estimated by using a lightwave component analyzer (Keysight).

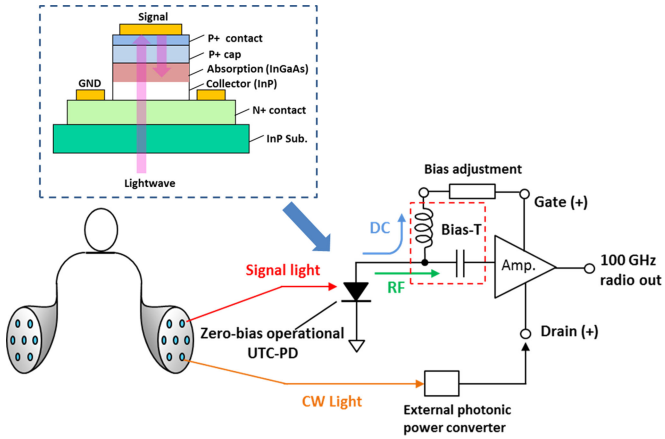

Fig. 2 Schematic diagram of 100 GHz optical-to-radio converter using power-over-fiber, and the layer structure of the zero-bias operational UTC-PD (upper inset).

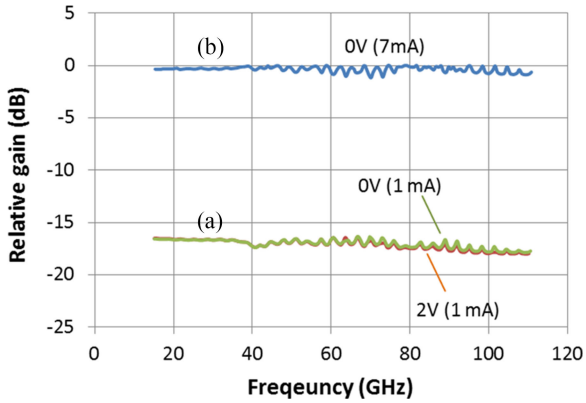

Fig. 3 (a) Frequency responses at 0 V/ 2 V at 1 mA photocurrent, and (b) 7 mA photocurrent at 0 V.

C. Electric Power Generation in UTC-PD

Subsequently, we estimated the DC electric power characteristics of UTC-PD, where the generated *I–V* curve should be defined by the built-in potential and the photocurrent from the optical input power. In the optical input power range of 1 mW to 10 mW at the wavelength of 1.55 μm, the *I–V* curve was measured with a commercially available variable resistor. Note that the variable resistor was used for the *I–V* curve measurement

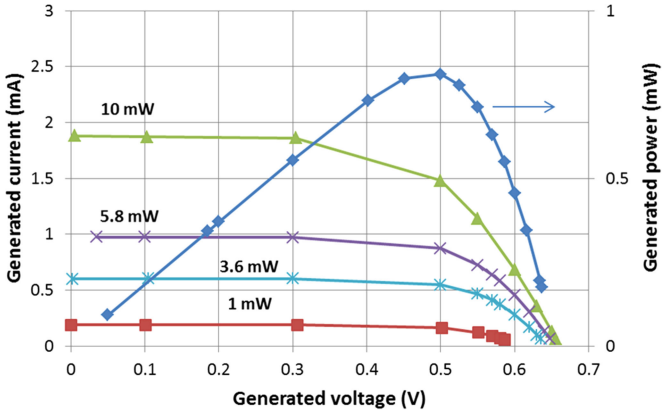

Fig. 4 Generated *I–V* curve and electric power in UTC-PD as a function of input power. The generated power (blue curve) was obtained at an input power of +10 dBm.

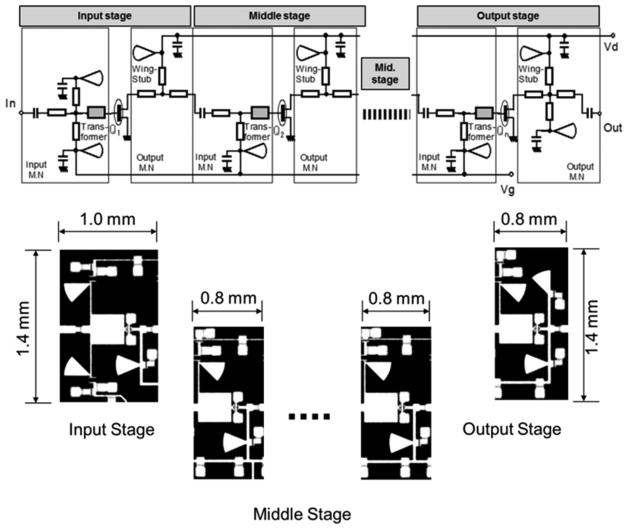

Fig. 5 The schematic circuit diagram (upper) and the photograph of fabricated 100 GHz range amplifier using enhancement mode PHEMT (lower).

and was not applied for the hybrid integration. Fig. 4 shows the generated DC current and voltage curve in UTC-PD. By increasing the resistor from 0 to high resistance, the photocurrent was down to approximately 0 mA, with a maximum voltage of 0.65 V. At optical input power of 10 mW, the generated maximum power and optical-to-electrical conversion efficiency was high as 0.74 mW and 7.4%, respectively [20]. The maximum input power of the UTC-PD at 0 V was measured as high as 45 mW so as to preserve the good output linearity.

D. Enhancement Mode 100 GHz Range PHEMT

A p-layer top structure with n-layer ground in the UTC-PD provides positive photocurrent to the gate bias in the PHEMT amplifier. Therefore, an enhancement mode PHEMT device, which can be operated in the positive bias region, would be required instead of depletion mode PHEMT devices. Although PHEMT devices are commonly operated in depletion mode, it is known that the depletion/enhancement mode operation in PHEMT devices is affected by the fabrication conditions [21], [22]. The depletion layer conditions in the Schottky barrier between the Schottky metal and semiconductor layer in PHEMT structure should affect the depletion/enhancement mode, and is affected by the semiconductor process conditions such as the semiconductor gate layer thickness and annealing process condition. Consequently, the drain-source current in a 2-dimensional channel layer strongly depends on the gate bias condition. We selected an enhancement mode PHEMT amplifier from the characteristic variations on a whole wafer.

We employed an InP based 0.1 μm PHEMT fabrication process, and the selected enhancement mode PHEMT exhibited gate applied bias voltage of +0.05 V to +0.2 V. The amplifier with the range of 100 GHz consisted of three parts, a transformer circuit for impedance matching on the input side, 4-stage amplifier in the middle, and conventional matching circuit on the output side as shown in Fig. 5. Here, we designed a unit amplifier that reduces the impact on the frequency characteristics even if the gain is increased by increasing the number of stages of amplifiers. Because each unit has several gain stages, an RF gain of approximately 20 dB can be obtained from the

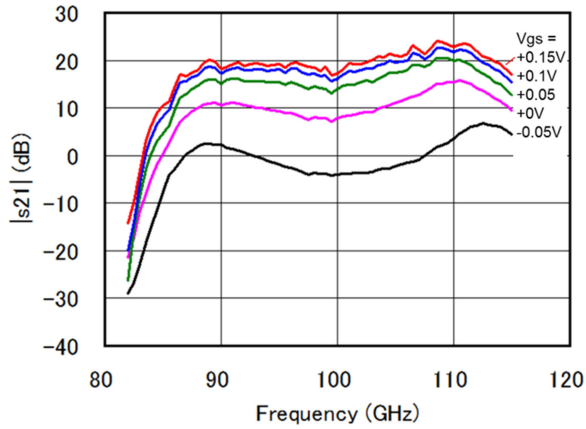

Fig. 6 Frequency response dependence of the gate bias voltage in 80–120 GHz.

4-stage units. Comparing the power consumption (few μW) of the gate as the load to that (0.8 mW) of UTC-PD, we realized the possibility of driving the gate bias using UTC-PD. Fig. 6 shows the frequency response (S21) dependence of the gain bias voltage ($V_g = -0.05$ to +0.15 V) at the external drain bias voltage $V_d = +1.4$ V (drain current $I_d = 50$ mA). In the frequency range of 88–112 GHz, the same curve and behaviors could be confirmed with a gain of −4 to +22 dB. The maximum output saturation power level was as high as +6 dBm at 95 GHz.

E. Optical-to-Radio Converter Module

Using the aforementioned key components, a hybrid integrated optical-to-radio converter was fabricated and tested under on-wafer conditions. Fig. 7 shows the RF output characteristics at 97 GHz as a function of the gate bias voltage, where the input photocurrent of 1 mA and the drain voltage of +1.4 V were supplied. The external bias feeds for drain and gate were used. Changing the gate bias voltage from the negative to the positive region, it was observed that the RF output of −2.5 to +1 dBm could be increased up to +2 to +5.5 dBm. Fig. 8

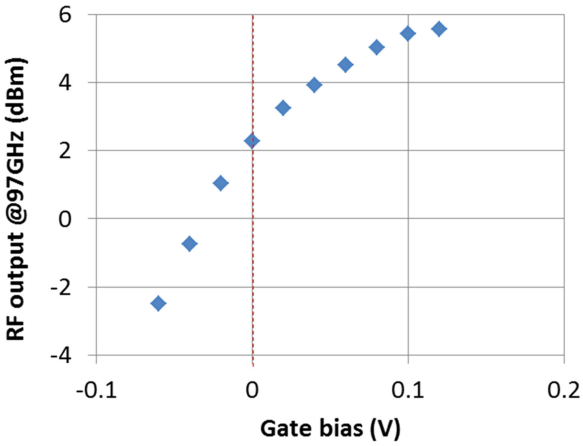

Fig. 7 RF output characteristics at 97 GHz as a function of gate bias voltage in the integrated photoreceiver.

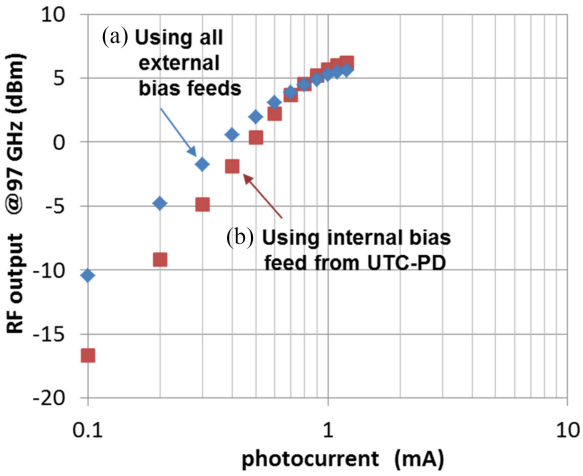

Fig. 8 The relationship between input photocurrent and RF output at 97 GHz, (a) using all external bias feeds, (b) using internal bias feed from UTC-PD.

shows the relationship between the input photocurrent and RF output at 97 GHz. Fig. 8(a) and (b) indicate the output properties, using (a) all external bias feeds, and (b) external drain bias feed with internal gate bias feed by UTC-PD. Different RF power increasing rates were seen in the photocurrent region of 0.1–1 mA, because the resistance of the variable resistor was fixed at a photocurrent of 1 mA for (b). However, good linearity and similar power saturation levels could be maintained for both conditions. When we implemented the hybrid integrated device into a metal package attached with a W-connector, an RF insertion loss of 4 dB was observed at 90–110 GHz, due to the impedance miss-matching between the RF output in the amplifier and the connector in the package. Then, the maximum power level at 97 GHz was down to +1.5 dBm.

III. Radio and Power Over Fiber Transmission Through Multi-Core Fiber For Multi-Point Access

Subsequently, we demonstrated RoF + PoF transmission through a multi-core fiber by considering point-to-multi-point access links. Fig. 9 shows the experimental setup. First, four-multiplied optical two-tone signals ($\lambda = 1549.3$ nm) were

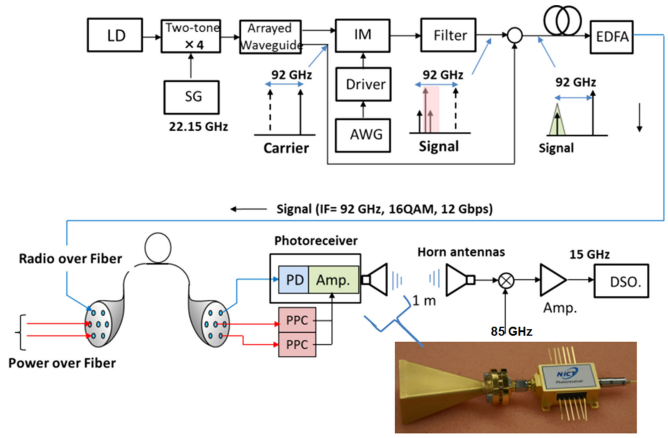

Fig. 9 Experimental setup for radio- and power-over-fiber transmission through multi-core fiber, (IF = 92 GHz, 12 Gbps OFDM 16-QAM).

prepared with an RF input of 22.15 GHz to an intensity modulator. The four-multiplied two-tone signals of 88.6 GHz were used as the high signal-to-noise ratio (SNR) intermediated frequency (IF) carrier, and were separated to the upper-side and lower-side bands by an arbitrary waveform generator (AWG). The lower-side band was modulated by an intensity modulator (IF = 3.5 GHz, 12 Gbps, 16-QAM, orthogonal frequency division multiplexing or OFDM), where the upper-side band was directly coupled to one of the optical coupler inputs without any modulation. The sub-upper sideband created in the main lower sideband was filtered out with the main lower sideband (see inset of the schematic optical spectrum in the upper part in Fig. 9) by using an optical narrow band-pass filter. After combining the remaining sub-lower sideband signal and un-modulated main upper-side band signal via an optical coupler, a 12 Gbps OFDM signal with IF = 92 GHz could be obtained. The signal of 12 Gbps was fed to an optical input in the integrated photo-receiver module. Two external photonic power converters (PPCs) were required for a PoF transmission, owing to the low O/E conversion efficiency. Notably, the photonic converter will become a single one, when the high efficiency PPC is considered. In this demonstration of RoF + PoF transmission, single-core RoF transmission and two-core PoF transmission conditions in 7-core fiber were adopted with the same wavelength (1549.3 nm). In the typical setup conditions, the two CW lightwaves of +23 dBm were supplied to the PoF, and the RoF signal power was varied from 0 to +4 dBm. After 1 m wireless transmission, the signal was down-converted to an IF of 7 GHz, and was analyzed in terms of bit error rate (BER) and error vector magnitude (EVM) by a high-speed oscilloscope.

Furthermore, in order to clarify the crosstalk issues in multi-core fiber, we compared the BER and EVM results with those of single mode fibers (three single mode fibers in total). Further, three single mode fibers were used for a single RoF transmission and two PoF transmissions as shown in Fig. 10(a). The same optical power conditions (+23 dBm in PoF, 0 to +4 dBm in RoF) as described above (7-core fiber) were utilized. Additionally, to enhance the crosstalk in RoF transmission, two more dummy PoF fibers at +23 dBm were attached to the 7-core fiber. Therefore, four cores were occupied with CW lightwave of +23 dBm

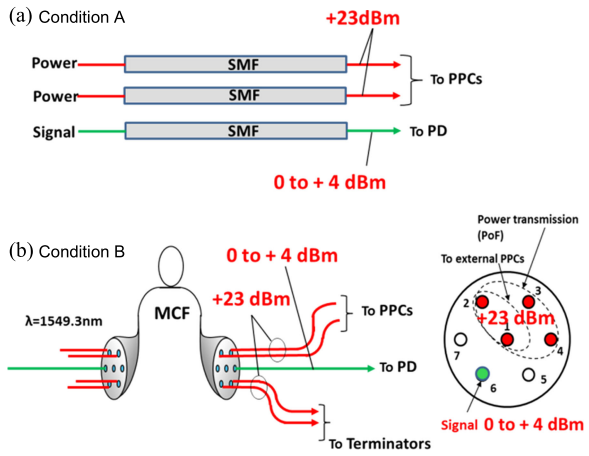

Fig. 10 Experimental conditions for RoF and PoF, (a) condition A: using 3-single mode fibers, (b) condition B: using 7-core fiber and the core locations of RoF and PoF.

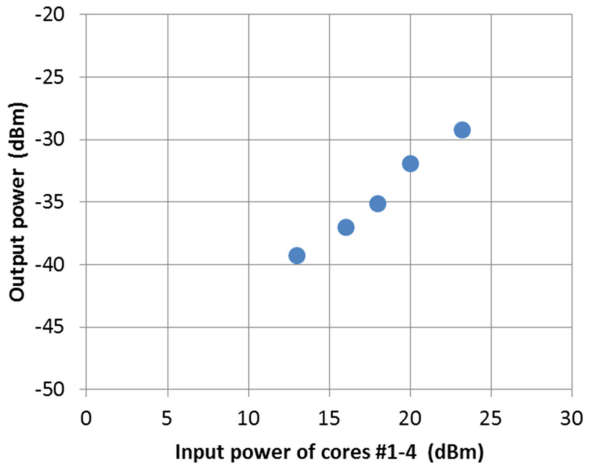

Fig. 11 The crosstalk measurement result in core #6 as a function of each optical power in core #1–4.

during the single core signal transmission. The cores located in #6 and #1–4 were used for RoF and PoF transmissions, respectively (as shown in Fig. 10(b)), with the specifications of core pitch of 45 μm and crosstalk of 40 dB.

Fig. 11 shows the crosstalk measurement result in #6 core as a function of optical power in each of the #1–4 core. At +13 dBm in each core (#1–4), low leakage power of −39 dBm was measured at 1549.3 nm. Since the crosstalk in #6 core was proportional to the input power (#1–4), −29 dBm in #6 core could be measured at +23 dBm in each core (#1–4), where the electric power of 50 mW required to drive the drain bias could be obtained from two CW lightwaves of +23 dBm. The power level of −29 dBm would be sufficiently low to enable RoF transmission at the power level of 0 to +4 dBm since the crosstalk is approximately 30 dB lower than the RoF signal.

Fig. 12 shows the estimated EVM and BER results through PoF + RoF transmission under both experimental conditions (A, B) in Fig. 10. A representative 16-QAM constellation diagram at +4 dBm RoF and +23 dBm PoF is shown in Fig. 12(a). The small EVMs of the range of 14% could be confirmed from

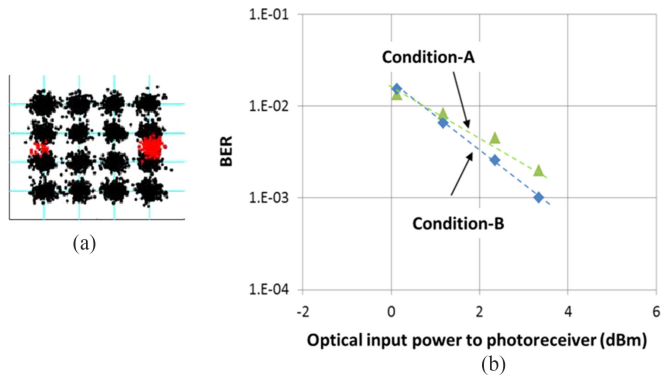

Fig. 12 (a) Constellation eye diagram with condition B, and (b) BER measurement results of 12 Gbps RoF and PoF transmission through 7-core fiber, condition A: using 3-single mode fibers, and condition B: using 7-core fiber and the core locations of RoF and PoF.

both the conditions. By changing the input power level to the integrated photoreceiver in RoF, the BER was measured (shown in Fig. 12(b)). No significant difference between the BER properties of these two conditions could be observed, where we speculated that the small difference was caused by the measurement error. For condition B (RoF + PoF), BER of 1×10^{-3} could be obtained at +3 dBm. Considering an overhead of 7% in forward error correction in order to obtain error-free condition, high data rate RoF transmission of 11.2 Gbps can be expected.

IV. Radio-Over-Fiber Transmission Through Multi-Core Fiber Using Single Zero-Biased UTC-PD For Point-to-Point Access

Regarding the related technology of Sections I–III, we demonstrated 100 GHz range RoF communication through a multi-core fiber using a single UTC-PD with zero-bias operation, integrated without the RF amplifier, by assuming another possible scenario for short distance point to small-scale cells communication. Introducing a high power 100 GHz range signal to the UTC-PD directly, a radio signal would be launched without any internal and external bias feeds. Subsequently, the transmission system configuration becomes very simple, and the fiber resources for PoF in the multi-core fiber can be reduced. Although long-range wireless communication distance might not be desired for the single UTC-PD at zero bias, compared to the integrated photoreceiver, it has potential applications for small-scale front-haul systems.

In Fig. 13, the experimental setup configuration at the transmitter side was the same as the one in Fig. 9. At the receiver side, the integrated photoreceiver was replaced by the single UTC-PD. Assuming five-core based RoF transmissions, an OFDM signal of 12 Gbps with four CW lightwaves as dummy signals, one of +10 dBm and four of +23 dBm, were introduced into the 7-core fiber, in order to enhance the crosstalk between cores. An optical signal with IF of 92 GHz was received by the UTC-PD, and the radio launched signal was down-converted to low frequency after 0.5 to 1.5 m wireless transmission. Fig. 14 shows the single sideband phase noise characteristics with/without dummy lightwaves from 4-core,

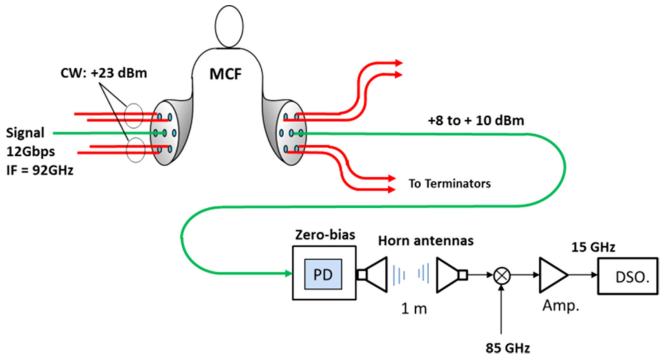

Fig. 13 Experimental setup condition using single zero-bias operational UTC-PD assuming 5-parallel RoF transmission through multi-core fiber.

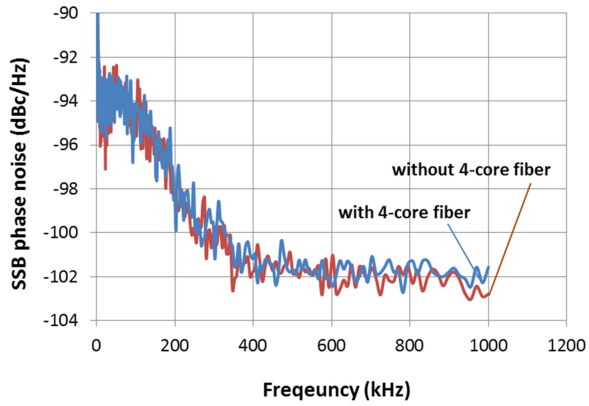

Fig. 14 SSB phase noise measurement result for single RoF and with 4-additional CW lightwave transmission.

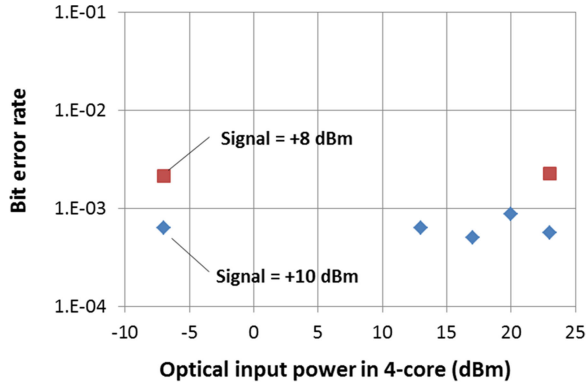

Fig. 15 Measured BERs at +8 dBm and +10 dBm signal power as a function of 4-additional CW lightwave power.

under the back-to-back (no wireless communication) condition. Comparing 12 Gbps signal spectra with/without the four lightwaves of +23 dBm, phase noise of −95 dBc/Hz at the offset of 100 kHz and −102 dBc/Hz at the offset of 500 kHz could be obtained for both conditions. It indicates that the minimum crosstalk affections from 4-core to the signal line (core) can be predicted.

With a 4-core dummy lightwave, RoF transmission was demonstrated under 0.5 m wireless communication. When the BER was measured, a value of 1×10^{-3} could be confirmed at the optical signal of +8.4 dBm as shown in Fig. 15. Moreover, the BERs were estimated at signal inputs of +8 dBm and +10 dBm, as a function of the optical power in 4-core (Pin4). At the signal power of +10 dBm, BER of 6×10^{-4} was observed at $\mathrm{Pin4} = +\ 0$ dBm, and it relatively increased with the Pin4. However, BER of 1×10^{-3} was maintained up to $\mathrm{Pin4} = +23$ dBm. At the signal power of +8 dBm, the same BER (2×10^{-3}) could be obtained from $\mathrm{Pin4} = +0$ dBm and +23 dBm. Subsequently, no BER degradation could be observed.

When we compared the signal input powers for the integrated photoreceiver and single zero-bias operational UTC-PD at BER of 1×10^{-3} under 1 m wireless transmission RoF, they were +10 dBm and +1.7 dBm, respectively. Subsequently, an attribution of 8.3 dB from the RF amplifier in the integrated photoreceiver was estimated. While eliminating the RF insertion loss of 4 dB at 90–110 GHz in the implementation of the photoreceiver in Section II-E, an attribution of 12.3 dB from the RF amplifier is expected.

V. Conclusion

In this report, a new approach of a high-speed photodetector based on electric power generation was described. Then, we designed and fabricated 100 GHz range integrated photoreceiver for power- and radio-over-fiber transmission through a multi-core fiber and elaborated the crosstalk issues. In the case of the integrated photoreceiver based on PoF transmission, an external electric power supply and an internal power supply from the UTC-PD were used through a multi-core fiber. In the demonstration of RoF-based wireless communication (IF = 92 GHz), high data rate transmission of 12 Gbps could be achieved below BER of 1×10^{-3}. With regards to the crosstalk issues in BER through PoF + RoF, the minimum penalty from PoF could be observed in the integrated photoreceiver. When the crosstalk in single zero-biased UTC-PD was measured by assuming five parallel RoF transmissions, no crosstalk affections could be observed with a BER of 1×10^{-3}.

Reference

[1] G. Raybon *et al.*, "Single carrier high symbol rate transmitter for data rates up to 1.0 Tb/s," in *Proc. Opt. Fiber Commun. Conf. Exhib.*, 2016, Paper Th3A.2.

[2] G. Khanna *et al.*, "Single-carrier 400G 64QAM and 128QAM DWDM field trial transmission over metro legacy links," *IEEE Photon. Technol. Lett.*, vol. 29, no. 2, pp. 189–192, Jan. 2017.

[3] M. V. Nichita, P. Ciotirnae, R. L. Luca, and V. N. Petrescu, "5G propagation: Current solutions and future proposals," in *Proc. 2006 12th IEEE Int. Symp. Electron. Telecommun.*, 2016, pp. 47–50.

[4] G. K. Chang and L. Cheng, "Fiber-wireless integration for future mobile communications," in *Proc. 2017 IEEE Radio Wireless Symp.*, 2017, pp. 16–18.

[5] Y. Sasaki *et al.*, "Crosstalk-managed heterogeneous single-mode 32-core fiber," in *Proc. 42nd Eur. Conf. Exhib. Opt. Commun.*, Dusseldoft, Germany, Sep. 2016, pp. 550–552.

[6] J. Sakaguchi *et al.*, "Large spatial channel (36-Core × 3 mode) heterogeneous few-mode multicore fiber," *J. Lightw. Technol.*, vol. 34, no. 1, pp. 93–103, Jan. 2016.

[7] T. Kobayashi *et al.*, "1-Pb/s (32 SDM/46 WDM/768 Gb/s) C-band dense SDM transmission over 205.6-km of single-mode heterogeneous multi-core fiber using 96-Gbaud PDM-16QAM channels," in *Proc. Opt. Fiber Commun. Conf. Exhib.*, 2017, Paper Th5B.1, Post-deadline-paper.

[8] J.-X. Cai *et al.*, "70.4 Tb/s capacity over 7,600 km in C+L band using coded modulation with hybrid constellation shaping and nonlinearity compensation," in *Proc. Opt. Fiber Commun. Conf. Exhib.*, 2017, Paper Th5B.2, Post-deadline-paper.

[9] T. Umezawa, K. Kashima, K. Akahane, A. Kanno, N. Yamamoto, and T. Kawanishi, "100 GHz fiber-fed optical-to-radio converter," in *Proc. 2016 Conf. Lasers Electro-Opt.*, 2016, Paper JTh4C.5, Post-deadline-paper.
[10] Application note in Lumentum product guide, "Powering remote data links over fiber." 2015. [Online]. Available: www.lumentum.com
[11] Huawei Technologies Co., "5G: A technology vision," 2013.
[12] J. G. Andrews *et al.*, "What will 5G be?" *IEEE J. Sel. Areas Commun.*, vol. 32, no. 6, pp. 1065–1082, Jun. 2014.
[13] T. S. Rappaport *et al.*, "Millimeter wave mobile communications for 5G cellular: It will work!," *IEEE Access*, vol. 1, pp. 335–349, 2013.
[14] C. T. Tsai, Y. C. Chi, P. C. Peng, and G. R. Lin, "Long-reach MMWoF using single-sideband modulated dual-mode VCSEL with 16-QAM OFDM at 8 Gbit/s," in *Proc. Opt. Fiber Commun. Conf. Exhib.*, 2017, Paper Tu2F.3.
[15] T. Thomas, K. Veeraswamyy, and G. Charishma, "5G mobile handset multi, wideband antenna with inductor operating at mm wave: Design and analysis," in *Proc. 2015 1st Int. Conf. Next Gener. Comput. Technol.*, Dehradun, India, Sep. 2015, pp. 551–554.
[16] Federal Communications Commission Office of Engineering and Technology, "Millimeter wave propagation: Spectrum management implications," Bulletin Number 70, Jul. 1997. [Online]. Available: https://transition.fcc.gov/Bureaus/Engineering_Technology/Documents/bulletins/oet70/oet70a.pdf.
[17] T. Umezawa *et al.*, "100-GHz fiber-fed optical-to-radio converter for radio- and power-over-fiber transmission," *IEEE J. Sel. Topics Quantum Electron.*, vol. 23, no. 3, May./Jun. 2017, Art. no. 3800508.
[18] T. Umezawa *et al.*, "Bias-free operational UTC-PD above 110 GHz and its application to high baud rate fixed-fiber communication and W-band photonic wireless communication," *J. Lightw. Technol.*, vol. 34, no. 13, pp. 3138–3147, Jul. 2016.
[19] T. Umezawa, K. Akahane, A. Kanno, N. Yamamoto, and T. Kawanishi, "Bias free operational 107-Gbaud ultra-fast photodetector," in *Proc. Eur. Conf. Opt. Commun.*, 2015, Paper P.2.3.
[20] T. Umezawa *et al.*, "100 GHz optical-to-radio converter module and its application in radio and power over fiber transmission through multi-core fiber," in *Proc. Opt. Fiber Commun. Conf. Exhib.*, 2017, Paper W4B.2.
[21] C.-K. Lin, J.-C. Wu, W.-K. Wang, H.-C. Chiu, and Y.-J. Chan, "The fabric enhancement-mode metamorphic InAlAs/InGaAs HEMT by Pt Schottky metal diffusion," in *Proc. Int. Conf. Solid State Devices Mater.*, Tokyo, Japan, 2003, pp. 664–665.
[22] A. J. Ping *et al.*, "Enhancement–mode InAlAs/InGaAs/InP high electron mobility transistor with strained InAlAs barrier layer," *Chin. Phys. Lett.*, vol. 17, no. 8, pp. 619–620, 2000.

Toshimasa Umezawa received the B.E. and M.E. degrees in electronics from Nagaoka University, Niigata, Japan, in 1984 and 1986, respectively, and the Ph.D. degree in electronics in 1995 from Tokyo University, Tokyo, Japan, where he was engaged in research on superconductor devices, photonics devices, and their applications. From 1987 to 2011, he worked for the Yokogawa Electric Corporation; he was in the Central Research Laboratory and in the Photonics Business Department. In 1992, he was a Visiting Scholar in the Department of Applied Physics, Stanford University. In 2011, he joined the National Institute of Information and Communications Technology, Tokyo, Japan. His research interests include E/O devices and photonic integrated circuits and millimeter-wave photonics.

Pham Tien Dat (M'12) received the B.Eng. degree in electronics and telecommunication engineering from the Posts and Telecommunications Institute of Technology, Ho Chi Minh City, Vietnam, and the M.Sc. and Ph.D. degrees in science of global information and telecommunication studies from Waseda University, Tokyo, Japan, in 2003, 2008, and 2011, respectively. He joined the National Institute of Information and Communications Technology, Japan, in 2011. His research interests include microwave/millimeter-wave photonics, radio over fiber, and optical wireless systems.

Kenichi Kashima received the B.E. degree in electronics from Hosei University, Tokyo, Japan, in 1993. From 1994, he worked for the Hitachi Kokusai Electric Inc. His research interests include millimeter-wave semiconductor devices and its application to wireless communication systems.

Atsushi Kanno (M'11) received the B.S., M.S., and Ph.D. degrees in science from the University of Tsukuba, Tsukuba, Japan, in 1999, 2001, and 2005, respectively. In 2005, he was in the Venture Business Laboratory, Institute of Science and Engineering, University of Tsukuba, where he was engaged in research on electron spin dynamics in semiconductor quantum dot structures using the optical-polarization-sensitive Kerr effect measurement technique. In 2006, he joined the National Institute of Information and Communications Technology, Japan. His research interests include microwave/millimeter-wave/terahertz photonics, ultrafast optical and radio communication systems, lithium niobate optical modulators, and ultrafast phenomena in semiconductor optical devices. He is a member of the Institute of Electronics, Information, and Communication Engineers, and the Japan Society of Applied Physics.

Naokatsu Yamamoto received the Ph.D degree in electrical engineering from Tokyo Denki University, Tokyo, Japan, in 2000. In April 2001, he joined the National Institute of Information and Communications Technology (NICT). In May 2008, he was a Visiting Professor in Tokyo Denki University and, from July 2012 to September 2013, the Deputy Director in the Ministry of Internal Affairs and Communications. Since 2016, he has managed a Network Science and Convergence Device Technology Laboratory in the NICT and also has been the Director of Advanced ICT Device Laboratory. His research interests include a heterogeneous quantum dot laser with silicon photonics, and a convergence device technology of photonics and wireless. Recently, he has also interested in the use of a 1.0-μm waveband (thousand-band, T-band) as a new optical frequency band for short-range communications.

Tetsuya Kawanishi (M'06–SM'06–F'13) received the B.E., M.E., and Ph.D. degrees in electronics from Kyoto University, Kyoto, Japan, in 1992, 1994, and 1997, respectively. From 1994 to 1995, he was in the Production Engineering Laboratory, Panasonic. In 1997, he was in the Venture Business Laboratory, Kyoto University, where he was engaged in research on electromagnetic scattering and near-field optics. In 1998, he joined the Communications Research Laboratory, Ministry of Posts and Telecommunications (now the National Institute of Information and Communications Technology (NICT)), Tokyo, Japan, where he is currently the Director of the Lightwave Devices Laboratory, NICT. In 2004, he was a Visiting Scholar in the Department of Electrical and Computer Engineering, University of California at San Diego. His research interests include high-speed optical modulators and RF photonics.